ICMIEE22-011

Effects of Impinging Distance, Reynolds Number, and Swirl on the Flow and Heat Transfer Behaviors of Arrays of Circular Impinging Jets: A Numerical Approach

Md. Tanvir Khan[1], Sudipta Debnath[2,], Zahir U. Ahmed[2], Sharif M. Islam[2]*
[1] Department of Mechanical and System Engineering, Okayama University, Okayama (700-0081), JAPAN
[2] Department of Mechanical Engineering, Khulna University of Engineering & Technology, Khulna-9203, BANGLADESH

ABSTRACT
Impinging air jets have enormous applications in heating and cooling industries, such as turbine blades electrical equipment, etc. Heat transfer under impinging jet is generally superior to conventional methods since the fluid flow in the form of jet impingement drastically increases its momentum. The interaction between the multiple jet arrangement and low to high swirl intensity warrants extensive research to achieve uniform heat transfer. This study examines both the inline and staggered arrangements of numerous round swirling air jets impinging vertically on a flat surface. In this regard, three-dimensional simulations are executed using the finite volume method for a number of control parameters such as Reynolds number (Re = 11600, 24600, and 35000), impingement distance (H/D = 1, 2, 3 and 4) and jet-to-jet spacing (Z/D = 1.5 and 3.0), while, D is considered as the diameter of the nozzles. The nozzles are arranged in both inline and staggered conditions to obtain the most effective heat transfer. The pressure distribution, wall temperature, and Nusselt number are investigated for different operating conditions. It is observed that the staggered array of nozzle arrangement shows better heat transfer performance than the inline arrangement. Moreover, the thermal performance increases with the Reynolds number and swirl number since the fluid velocity as well as heat transfer rate increase due to turbulence. Besides, higher spacing between neighboring jets secures greater cooling areas on the impinging plate and accelerates the procedure to gain better uniformity in cooling effect. However, the thermal performance compromises with increasing impingement distance since much interaction time are involved in case of higher traveling distance.

Keywords: CFD, Jet Impingement, Swirl Flow, Turbulence, Heat transfer.

1. Introduction
Jet impingement is considered a promising technique to enhance heat transfer due to acceleration in turbulence in the jet surrounding fluid [1]. The local heat transfer coefficient at the jet stagnation zone is high because of the formation of thin boundary layers. Due to the design simplicity, low cost, as well as coherent heat and mass transfer properties, jet impingement is extensively utilized in a plethora of industrial applications that aim to achieve intense heating, cooling, or drying rates. Some common applications include the paper industry, cooling, and heating in the food industry, cooling of gas turbine blades, electronic devices, etc. [2-7].

The higher convective heat transfer rate of jet impingements ensures immediate cooling or heating of the target surface. Single-impinging jets have verified their prospects for considerable industrial exercises; however, most industrial applications demand immediate heat transfer from extended regions. Numerous impinging jets may be a suitable option in this regard because of the notable interchanges among the jets and correlated mixing. Moreover, the application of swirl in such complicated jet interaction may ameliorate or exacerbate the thermofluidic behavior and it requires to be resolved for an adequate knowledge of the integrated effects on the heat transfer performance. A number of research on impinging jets have been carried out over the last couple of decades due to their extensive applications in industrial sectors. Some of the relevant literature is discussed for brevity.

Tepe et al. [8, 9] investigated the flow and heat transfer behavior of jet impingement for various geometrical parameters under turbulent flow conditions and found that the SST k-ω turbulence model accurately predicts the experimental data. Moreover, the average Nusselt number is found to increase up to 40.32% by using extending the jet holes towards the target surface. The local Nusselt number increment is inversely proportional to the impinging distance and low towards the streamwise direction due to the cross-flow augmentation. Besides, the thermal stress on the target surface can be reduced by decreasing the impinging distance. The heat transfer rate accelerates with the jet velocity but starts decreasing after the potential core region due to the shear stress of the fluid. Moreover, the rib design is found a paramount parameter of thermal performance and the improper rib design can diminish the heat transfer performance. Chang and Shen [10] found that the heat transfer rate significantly reduces at a low impingement distance due to the flow confinement between the smooth nozzle-containing plate and the impinging surface. However, for a high impingement distance, the additive ambient fluid entrainment from the grooves accelerates the jet momentum to boost the heat transfer level. Vinze et al. [11] investigated the effect of dimple pitch and depth on jet impingement heat transfer over a dimpled surface and found that for smaller pitches, the flat plate is more efficient than a dimpled surface. However, for greater pitches, the dimpled surface performed much better in comparison with the flat plate. Pachpute and Premachandran [12] conducted experimental and numerical studies of a set of inline and staggered air jet impingement on a circular cylinder for different flow conditions and found that the staggered

* Corresponding author. Tel.: +88-01893928518
E-mail address: sudiptadebnath913@gmail.com

layout of jets enhances the rate of cooling compared to the inline layout for lower impinging distance, however, for the higher impinging distance, the average Nusselt numbers of the staggered layout of jets are comparatively lower than that of the inline layout. Moreover, the local and average Nusselt number increase with decreasing the nozzle to plate distance. Singh and Prasad [13] studied the heat transfer performance of a set of staggered air jets using two configurations of (45°) chamfered and non-chamfered arrangement and found that the chamfered configuration performs better than its counterparts in terms of cooling coverage area, heat transfer enhancement, higher energy saving, and reduction in coolant requirement. The thermal performance of chamfered configuration is 8–24% better than that of the non-chamfered configuration for the same flow rate. Chen et al. [14] numerically studied the heat transfer performance of a staggered and inline array of jet impingement on a cubic micro pin fin roughened surface and found a 19% enhancement in the heat transfer rate due to the increased surface area. Moreover, the inline arrangement of the rib surface results in a higher Nusselt number compared to the staggered jet pattern. Kuntikana and Prabhu [15] observed that the heat transfer behavior of the isothermal air jet and the premixed flame jet are almost the same. The higher thermal entrainment in premixed flame jets results in lower effectiveness. Moreover, the potential core length of isothermal air jets and the premixed flame cone height of premixed flame jets play a significant role in jet impingement heat transfer. Penumadu and Rao [16] found that the CFD analysis overestimates the heat transfer coefficient and pressure drop. A large amount of pressure loss is found to occur due to the contraction effect at the nozzle entrance and loss of kinetic energy. The pressure drop also depends on the nozzle diameter significantly although independent of the impinging distance. The downstream jet that oscillates due to crossflow, affects the impinging jet significantly. A non-monotonic variation in the Nusselt number distribution is observed along the stream-wise direction since the cross-flow interacts and the jet velocity changes. Moreover, the upwash of the wall jets and primary vortices cause an enhancement in the local heat transfer at the upstream of the jets. Besides, jet clogging is found to adversely affect heat transfer and pressure drop. Satish and Venkatasubbaiah [17] found better heat transfer enhancement for multiple jet impingement compared to a single jet due to multiple recirculation zones and the heat transfer rate increases with the number of jets. However, a single jet enhances the heat transfer rate from the top surface of the block compared to multiple jets. Taghinia et al. [18] used RANS and LES models to investigate the pressure distribution and heat transfer of a twin-jet impingement and observed that the RANS model predicts the data accurately at a lower impinging distance while the LES model over-estimates the pressure value at some locations. Moreover, RANS is more suitable for predicting the peak values of local Nusselt numbers at correct locations. The pressure distribution is profoundly influenced by the nozzle-to-plate spacing and to some extent by the nozzle-to-nozzle spacing. The flow is found to expand radially with the impinging distance. Moreover, the second stagnation region expanded with the radial distance causing a jump in the local Nusselt number distribution. Yong et al. [19] found that for dense array jet impingement, the flow is more likely a channel flow due to the strong adjacent jet interference. The strong jet-induced crossflow deflects the downstream impinging jet and weakens the normal penetration of jet impingement, which cause a significant reduction in the convective heat transfer. The staggered arrangement is found superior to the inline arrangement in terms of heat transfer performance, however, the performance is compromised due to crossflow. Debnath et al. [20-22] numerically investigated the thermal performance of an array of multiple jet arrangements and found that the staggered nozzle arrangement shows better heat transfer performance. Moreover, thermal performance in swirl flow is more prominent compared to the no swirl flow. In this study, the mechanical and thermal performance are investigated numerically for different geometric arrangements and flow conditions, and the effect of these parameters is analyzed. Pressure distribution and heat transfer characteristics are observed for low to high Reynolds numbers and swirl numbers, and the effect of impinging distance, jet-to-jet separation distance, and nozzle arrangement are investigated.

2. Methodology

This study considers a multiple turbulent incompressible swirling air jet impinging perpendicularly onto a flat smooth plate. Twenty-five circular nozzles of diameter D (40 mm) are organized symmetrically with an axis into two different types of arrangements: inline and staggered. All the nozzles are evenly distributed into three concentric rings, around a central nozzle with 8 nozzles in each circle. The impinging distance is assumed H and the jet-to-jet spacing that varies with the concentric rings is Z. Only a quarter of the full domain is considered for the analysis to optimize computational cost. The physical arrangement of the nozzle with the coordinate system is represented in Fig.1. The jets originate from axial-plus-tangential aerodynamic swirl generators, where required swirl intensities are maintained for the identical mass flow rate. The details of the nozzle are described in the literature 23-26.

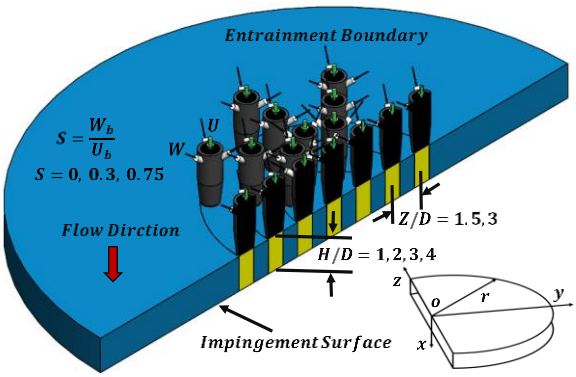

Fig.1 3D schematic diagram of the computational domain with nozzle arrangements.

The RANS model is employed to settle the flow and energy variables for the 3*D* problem. The governing equation in packed format is [27]:

$$\frac{\partial(\rho u\phi)}{\partial x}+\frac{\partial(\rho v\phi)}{\partial y}+\frac{\partial(\rho w\phi)}{\partial z}=\frac{\partial}{\partial x}\left(\Gamma_\phi\frac{\partial\phi}{\partial x}\right)+\frac{\partial}{\partial y}\left(\Gamma_\phi\frac{\partial\phi}{\partial y}\right)+\frac{\partial}{\partial z}\left(\Gamma_\phi\frac{\partial\phi}{\partial z}\right)+S_\phi$$

where ρ, ϕ, Γ_ϕ, and S_ϕ act for the air density, flow and temperature variables, effective transport coefficients, and source terms, individually.

The governing equations and transport equations are resolved using finite-volume-based commercial software ANSYS Fluent (v17). Velocity inlet boundary condition is employed at individual nozzle exit plane and the data for the required swirl intensities are achieved from Ahmed et al. [28]. No-slip and steady wall heat flux are implemented at the impinging plate, and the atmospheric pressure is selected at the inlet and outlet edges. The pressure inlet state is applied at the upper part of the computational domain (except the nozzle area) and the pressure outlet is selected at the outlet section. Symmetry and periodic conditions are applied at the two sides for non-swirling and swirling cases, respectively. The coupled solver is utilized for pressure velocity coupling, with Green-Gauss node-based gradient discretization and PRESTO for pressure discretization. Second-order discretization schemes are used for the convective terms and diffusion terms are solved by the second-order accurate (central difference) method. The solution is assumed converged when residuals of the variables reached down up to 10^{-05}.

Tetrahedral mesh (unstructured) mesh is applied to the computational domain. 15 inflation layers with a growth rate of 1.2 are used in the vicinity of the impingement surface to better resolved the flow phenomena as well as thermal performance. Due to insignificant flow variation, a comparatively coarser mesh is applied at the outer and upper edges of the computational domain. Mesh containing 818k nodes is used for the simulations. y+ values are ensured to less than one in the whole domain for both inline and staggered arrangements of jets. A typical mesh with boundary conditions is presented in Fig. 2.

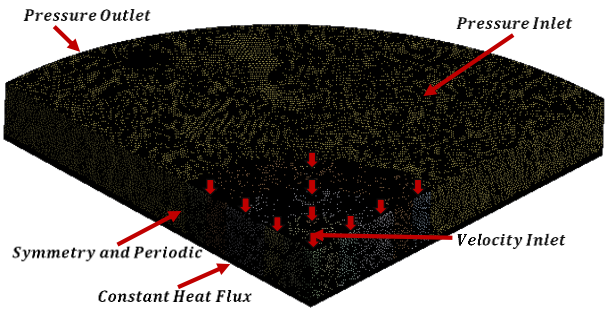

Fig.2 Grid generation and boundary conditions.

Turbulence model selection is very important for the accurate prediction of flow parameters. In this regard, three incompatible turbulence models (SST *k-ω*, Transition SST, and Realizable *k-ε*) are tested opposed to the experimental data. Fig. 3 represents the numerical predictions of skin friction coefficient (C_f) at impinging plate along the radial line in the horizontal direction for single nozzle medium swirl flow at *Re* = 35000 and *H* = 1*D*, using 3 different turbulence models and the corresponding experimental data [23]. It is observed that the skin friction coefficient predicted by the SST *k-ω* model is pretty similar to the experimental value while the Transition SST model predicts the skin friction coefficient accurately near the impingement zone, however, over-predicts at the downstream locations. On the contrary, Realizable *k-ε* overestimates the experimental data all over the domain. Finally, SST *k-ω* model is selected for the analysis due to its superiority in terms of predicting the experimental result.

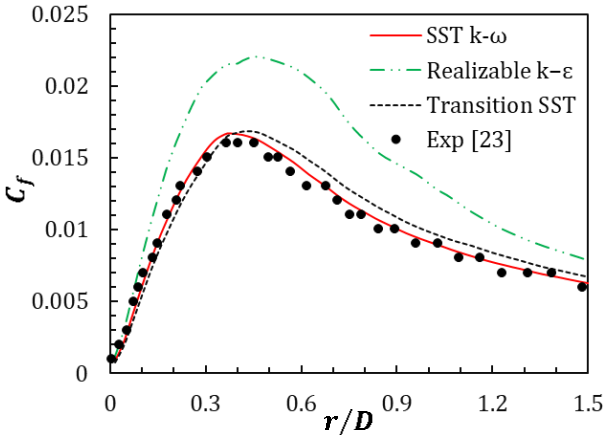

Fig.3 Radial distribution of skin friction coefficient (C_f) for single nozzle medium swirl flow at *Re* = 35000 and *H* = 1*D* for different turbulence models and the corresponding experimental data.

3. Result & Discussion

In this study, the nozzle emanated jet flow impinges on a heated plate for different flow conditions. To analyze the effects of the Reynolds number on the radial uniformity of wall pressure distributions, Fig. 4 represents the data for different swirl numbers (*S* = 0, 0.3, and 0.75), Reynolds number (*Re* = 11,600, 24600, and 35,000), and nozzle arrangements (inline and staggered) at an impinging distance of 2*D* (*H/D* = 2) and jet-to-jet spacing of 3*D* (*Z/D* = 3). The coefficient of pressure can't be used as a dimensionless parameter to compare pressures on impingement wall surfaces at different Reynolds numbers since the dynamic pressure is varying in each case. Therefore, the wall static pressure is normalized by the maximum pressure in the radial spread out for each given swirl number. The static pressure is found to be almost independent of Re for non-swirling (*S* = 0) and medium swirling (*S* = 0.3) jets at both inline and staggered arrangements of nozzles. Here, a slight variation in the normalized pressure is observed for *S* = 0 at *r/D*=7–9 and *r/D*=5–7 for the inline and staggered configurations, respectively. For inline array of medium swirling jets, variations are observed at *r/D*=4–4.5 and *r/D*=6–6.5. This deviation may be attributed to different characteristics of large-scale secondary vortex rings and their influences on the downstream flow development at

the impingement surface. Nevertheless, in case of higher swirl greater variations are observed for *Re* = 35000 from the results of *Re* = 11600 and 24600. These might be due to severer recirculation regions at the impinging plate for the strong swirl intensities in case of higher Reynolds number and swirl number.

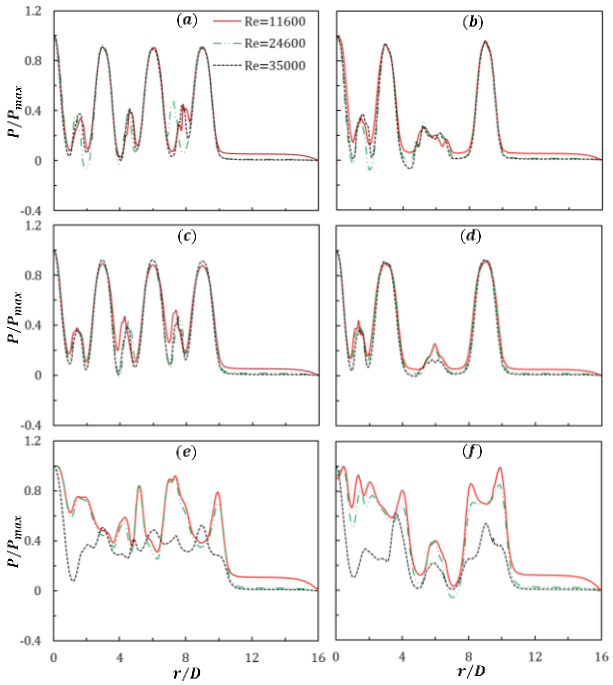

Fig.4 The effect of Reynolds number on impingement pressure distribution at *H/D* = 2 and *Z/D* = 3 at (a) Inline, *S* = 0; (b) Staggered, *S* = 0; (c) Inline, *S* = 0.3; (d) Staggered, *S* = 0.3; (e) Inline, *S* = 0.75 and (f) Staggered, *S* = 0.75.

Fig.5 represents the impinging wall temperature (T_w) distribution along the radial direction at inline and staggered arrangements of nozzle for different swirl numbers (*S* = 0, 0.3, 0.75) and impinging distances (*H* = 1*D* and 4*D*) at Reynolds number, *Re* = 11600 and jet-to-jet separation, *Z/D* = 3. For non-swirl and medium swirl conditions, medium peaks at temperature distribution are observed around *r/D* = 1-2, 4-5, and 7-8 regions for the inline nozzle arrangements at both impingement distances. Besides, a weak peak is also found around *r/D* = 9 in the case of smaller *H/D*. On the other hand, these regions are allocated around *r/D* = 1-2 and *r/D* = 5.5-7.5 for staggered arrays of nozzles. Moreover, these peaks appear stronger at a maximum impinging distance and staggered arrangement of nozzles. For higher swirl flows, different characteristics are observed in the temperature profiles. Stronger peaks are evident along with the weaker ones and temperature peaks increase significantly with the impinging distance. A uniform increment of T_w is found for all the cases from the *r/D* = 10 region. It is noticed that the temperature at the nozzle stagnation zones is low and farther from the stagnation zones the temperature is high. The peak of the temperature profile in between the nozzle stagnation zones asserted this observation. Moreover, after *r/D* = 10, no nozzle is located on the heated plate. So temperature is uniformly increasing with the radial distance from the nozzle arrangements. Therefore, a significant reduction in hot surface temperature distribution is evident at the nozzle locations which validates the jet impingement efficiency. It can be also observed from the figure that, maximum cooling is achieved at a minimum impinging distance, and with the increase of impinging distance, more uniformity is gained and cooling effects extend radially further. This is because when the impinging distance increase, the cold jet flow travels a longer distance until it meets the lower hot wall. As a result, the impact of fluid temperature on the wall decreases. Consequently, the cooling effect reduces while increasing the geometrical parameter *H/D*. Moreover, it is also observed that a higher swirl accelerates the process of getting more uniformity in temperature distribution and better cooling is achieved for the staggered arrangement of nozzles. This can be attributed to the fact that due to high swirl flow the turbulence in the flow field increases, so the fluid particle collides with each other, and their relative velocity increases, which accelerates the heat transfer. Consequently, better cooling performance is achieved with increasing swirl flow.

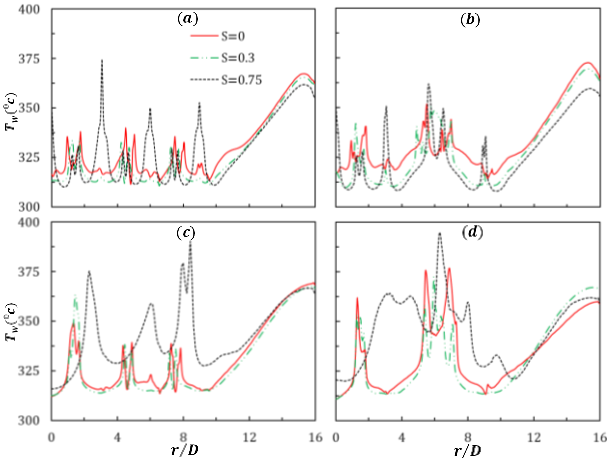

Fig.5 Radial distribution of wall temperature (T_w) for various swirling flows at *Z/D* = 3 and *Re* = 11600 at (a) Inline, *H/D* = 1; (b) Staggered, *H/D* = 1; (c) Inline, *H/D* = 4; (d) Staggered, *H/D* = 4.

Fig. 6 shows the average Nusselt number ($\overline{Nu}$) distributions at the impinging plane for different impinging distances (*H/D* = 1, 2, 3, 4), swirl numbers (*S* = 0, 0.3 & 0.75), and nozzle arrangements (inline and staggered) at a jet-to-jet separation of 1.5*D* (*Z/D* = 1.5). Here the circumferential area-averaged surface Nusselt number ($\overline{Nu}$) is derived for all cases using the formula: $\overline{Nu} = \frac{1}{A}\int Nu dA$, where *A* is the circumferential area on the impinging plate, and a circumferential area of radius 8*D* (*r/D* = 8) is chosen for the analysis. It is observed that the value of $\overline{Nu}$ decreases with the increase of impinging distance for the swirl flow since the cold fluid requires much time to interact with the hot surface. This effect increases proportionally with the swirl number as a higher swirl requires higher traveling time. On the other hand, in the case of no swirl flow, this behavior reverses

which might be due to the fact that the fluid velocity increases since the fluid is emitted directly from the nozzle. Consequently, the impact of the fluid becomes high. For low impinging distance, higher swirl flow results in $\overline{Nu}$ augmentation since the turbulence in the nozzle emanated fluid is high which eventually enhances the fluid velocity as well as the heat transfer rate. Moreover, the average Nusselt number sharply decreases for the staggered arrangement than the inline one for the high swirl condition since no cross flow occurs in the case of staggered arrangement.

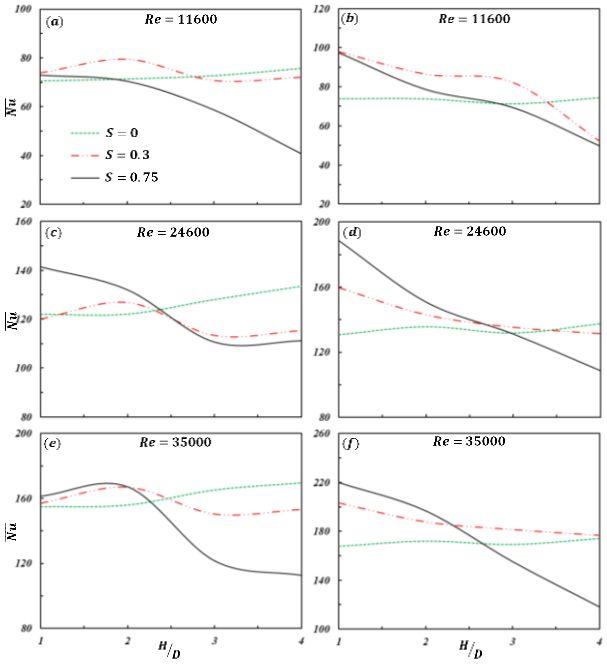

Fig.6 $\overline{Nu}$ Vs *H/D* for different swirl numbers when *Z/D* = 1.5 at (a) Inline, *Re* = 11600; (b) Staggered *Re* = 11600; (c) Inline, *Re* = 24600; (d) Staggered, *Re* = 24600; (e) Inline, *Re* = 35000 and (f) Staggered, *Re* = 35000.

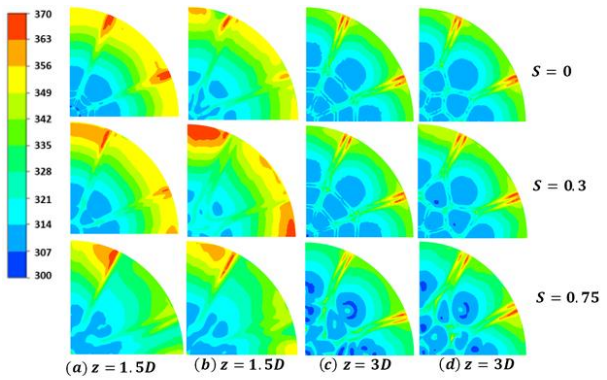

Fig.7 Wall temperature recorded on the heated plate for *Re* = 24600 at (a) Inline *H* = 2*D*, *Z* = 1.5*D*; (b) Staggered *H* = 2*D*, *Z* = 1.5*D*; (c) Inline *H* = 2*D*, *Z* = 3*D*; (d) Staggered *H* = 2*D*, *Z* = 3*D*.

Fig. 7 shows the wall temperature contours of the heated impingement plate for different swirl conditions (*S* = 0, 0.3 & 0.75), jet-to-jet separations (*Z/D* = 1.5, 3), and nozzle arrangements (inline and staggered) at a Reynolds number of 24600. It is observed that maximum cooling is obtained below the nozzles and between the nozzles where a strong recirculation region exists. Moreover, a comparatively better cooling is gained for the staggered arrangement of nozzles since no crossflow is generated. Greater jet-to-jet distance secures substantial cooling areas on the heated surfaces and higher swirl flows accelerate the procedure to gain better uniformity in the cooling effect, which is also substantiated by Debnath et al. [29].

4. Conclusion

This study numerically examines the thermofluidic aspects of inline and staggered arrangement of multiple swirling impinging jets. The influence of different flow and geometric parameters such as swirl number (*S* = 0, 0.3, and 0.75), Reynolds number (*Re* = 11,600, 24600 and 35000), impinging length (*H/D* = 1-4), and jet-to-jet separation length (*Z/D* = 1.5 and 3) on the pressure distribution and heat transfer behavior are investigated. The results are summarized as:

- Better heat transfer performance is observed in the case of the staggered array of nozzle arrangement since no cross flow occurs.
- The average Nusselt number decreases with the increase of impinging distance since the cold fluid requires much time to travel and interact with the hot surface.
- Swirl flow ensures better thermal performance since high turbulence is achieved, which in turn increases the fluid velocity as well as the heat transfer rate due to the rapid collision of fluid particles.
- The Nusselt number increases with the Reynolds number since the fluid velocity increases which accelerates the heat transfer rate.
- Higher jet-to-jet separation guaranteed greater cooling areas on the heated plate that accelerates the procedure to gain better uniformity in the cooling effect.

5. References

[1] Yadav, S., & Saini, R. P. (2020). Numerical investigation on the performance of a solar air heater using jet impingement with absorber plate. Solar Energy, 208, 236-248.

[2] Martin, H. (1977). Heat and mass transfer between impinging gas jets and solid surfaces. In Advances in heat transfer (Vol. 13, pp. 1-60). Elsevier.

[3] Ikhlaq, M., Al-Abdeli, Y. M., & Khiadani, M. (2019). Transient heat transfer characteristics of swirling and non-swirling turbulent impinging jets. Experimental Thermal and Fluid Science, 109, 109917.

[4] Yang, L., Ren, J., Jiang, H., & Ligrani, P. (2014). Experimental and numerical investigation of unsteady impingement cooling within a blade leading edge passage. International Journal of Heat and Mass Transfer, 71, 57-68.

[5] Ahmed, Z. U., Al-Abdeli, Y. M., & Guzzomi, F. G.

(2016). Heat transfer characteristics of swirling and non-swirling impinging turbulent jets. International Journal of Heat and Mass Transfer, 102, 991-1003.
[6] Son, C., Gillespie, D., Ireland, P., & Dailey, G. M. (2001). Heat transfer and flow characteristics of an engine representative impingement cooling system. J. Turbomach., 123(1), 154-160.
[7] Sarkar, A., Nitin, N., Karwe, M. V., & Singh, R. P. (2004). Fluid flow and heat transfer in air jet impingement in food processing. Journal of food science, 69(4), CRH113-CRH122.
[8] Tepe, A. Ü., Uysal, Ü., Yetişken, Y., & Arslan, K. (2020). Jet impingement cooling on a rib-roughened surface using extended jet holes. *Applied Thermal Engineering*, *178*, 115601.
[9] Tepe, A. Ü., Yetişken, Y., Uysal, Ü., & Arslan, K. (2020). Experimental and numerical investigation of jet impingement cooling using extended jet holes. International Journal of Heat and Mass Transfer, 158, 119945.
[10] Chang, S. W., & Shen, H. D. (2019). Heat transfer of impinging jet array with web-patterned grooves on nozzle plate. International Journal of Heat and Mass Transfer, 141, 129-144.
[11] Vinze, R., Khade, A., Kuntikana, P., Ravitej, M., Suresh, B., Kesavan, V., & Prabhu, S. V. (2019). Effect of dimple pitch and depth on jet impingement heat transfer over dimpled surface impinged by multiple jets. International Journal of Thermal Sciences, 145, 105974.
[12] Pachpute, S., & Premachandran, B. (2020). Turbulent multi-jet impingement cooling of a heated circular cylinder. International Journal of Thermal Sciences, 148, 106167.
[13] Singh, A., & Prasad, B. V. S. S. S. (2019). Influence of novel equilaterally staggered jet impingement over a concave surface at fixed pumping power. Applied Thermal Engineering, 148, 609-619.
[14] Chen, L., Brakmann, R. G., Weigand, B., Poser, R., & Yang, Q. (2020). Detailed investigation of staggered jet impingement array cooling performance with cubic micro pin fin roughened target plate. Applied Thermal Engineering, 171, 115095.
[15] Kuntikana, P., & Prabhu, S. V. (2016). Isothermal air jet and premixed flame jet impingement: heat transfer characterisation and comparison. International Journal of Thermal Sciences, 100, 401-415.
[16] Penumadu, P. S., & Rao, A. G. (2017). Numerical investigations of heat transfer and pressure drop characteristics in multiple jet impingement system. Applied Thermal Engineering, 110, 1511-1524.
[17] Satish, N., & Venkatasubbaiah, K. (2019). Numerical investigations of turbulent multiple jet impingement on a heated square block in a confined channel. Thermal Science and Engineering Progress, 14, 100415.
[18] Taghinia, J., Rahman, M. M., & Siikonen, T. (2014). Numerical investigation of twin-jet impingement with hybrid-type turbulence modeling. Applied Thermal Engineering, 73(1), 650-659.
[19] Yong, S., Jing-zhou, Z., & Gong-nan, X. (2015). Convective heat transfers for multiple rows of impinging air jets with small jet-to-jet spacing in a semi-confined channel. International Journal of Heat and Mass Transfer, 86, 832-842.
[20] Debnath, S., Khan, M. H. U., & Ahmed, Z. U. (2020). Turbulent swirling impinging jet arrays: A numerical study on fluid flow and heat transfer. *Thermal Science and Engineering Progress*, *19*, 100580.
[21] Debnath, S., Khan, M. H. U., Ahmed, Z. U., & Alam, M. M. The Effect of Swirl on Array of Turbulent Impinging Jets. In *International Conference on Mechanical, Industrial and Energy Engineering (ICMIEE2018)*.
[22] Debnath, S., & Ahmed, Z. U. Computational Analysis of Multiple Non-Swirling & Swirling Impinging Air Jets. In *International Conference on Mechanical, Industrial and Energy Engineering (ICMIEE2020)*.
[23] Ahmed, Z. U. (2016). An experimental and numerical study of surface interactions in turbulent swirling jets.
[24] Islam, S. M., Khan, M. T., & Ahmed, Z. U. (2020). Effect of design parameters on flow characteristics of an aerodynamic swirl nozzle. *Progress in Computational Fluid Dynamics, an International Journal*, *20*(5), 249-262.
[25] Khan, M. T., Islam, S. M., & Ahmed, Z. U. (2020). Near-wall and turbulence behavior of swirl flows through an aerodynamic nozzle. *Journal of Engineering Advancements*, *1*(2), 43-52.
[26] Khan, T., & Ahmed, Z. U. (2022). Effect of nanofluids on heat transfer characteristics of an aerodynamic swirl nozzle for isothermal and isoflux conditions. *Australian Journal of Mechanical Engineering*, 1-19.
[27] Ahmed, Z. U., Al-Abdeli, Y. M., & Guzzomi, F. G. (2017). Flow field and thermal behaviour in swirling and non-swirling turbulent impinging jets. *International Journal of Thermal Sciences*, *114*, 241-256.
[28] Ahmed, Z. U., Al-Abdeli, Y. M., & Guzzomi, F. G. (2015). Impingement pressure characteristics of swirling and non-swirling turbulent jets. *Experimental Thermal and Fluid Science*, *68*, 722-732.
[29] Debnath, S., Ahmed, Z. U., Ikhlaq, M., & Khan, T. Thermal characteristics of arrays of swirling impinging jets: Effect of Reynolds number, impingement distance, and jet‐to‐jet separation. *Heat Transfer*.

NOMENCLATURE

C_p : Pressure Coefficient
C_f : Skin Friction Coefficient
D : Nozzle diameter (40 mm)
H : Nozzle to plate distance (m)
Nu : Nusselt number (hD/k)
S : Swirl number (dimensionless), W_b/U_b
Z : Jet-to-jet separation distance (m)